Seasonal thermodynamic prediction of the performance of a hybrid solar gas-turbine power plant

M.J. Santos

Departamento de Física Aplicada, Universidad de Salamanca, 37008 Salamanca, Spain

R.P. Merchán

Departamento de Física Aplicada, Universidad de Salamanca, 37008 Salamanca, Spain

A. Medina *

Departamento de Física Aplicada, Universidad de Salamanca, 37008 Salamanca, Spain

A. Calvo Hernández

Departamento de Física Aplicada and IUFFYM, Universidad de Salamanca, 37008 Salamanca, Spain

Abstract

A thermodynamic model is developed for predicting the performance records of a solar hybrid gas turbine power plant with variable irradiance and ambient temperature conditions. The model considers a serial solar hybridization in those periods where solar irradiance is high enough. A combustion chamber allows to maintain an approximately constant inlet temperature in the turbine ensuring an stable power output. The overall plant thermal efficiency is written as a combination of the thermal efficiencies of the involved subsystems and the required heat exchangers. The model is validated by comparing its predictions against experimental results from a project developed near Seville, Spain. Real data for irradiance and external temperature are taken in hourly terms. The curves of several variables are obtained for representative days of all seasons: overall plant efficiency, solar subsystem efficiency, solar share, fuel conversion rate, and power output. The fuel consumption assuming natural gas fueling is calculated and the reduction in greenhouse emissions is discussed. It is shown that a recuperative hybrid plant configuration leads to a considerable saving of fuel consumption and emissions.

Key words: Thermosolar gas-turbines, Hybrid plants, Thermodynamic model, Variable solar irradiance, Global plant performance

PACS: 05.70.Ln, 07.20.Pe, 84.60.-h

* Corresponding author. Phone: +34 923 29 44 36; fax: +34 923 29 45 84
Email addresses: smjesus@usal.es (M.J. Santos), rpmerchan@usal.es (R.P. Merchán), amd385@usal.es (A. Medina), anca@usal.es (A. Calvo Hernández).

Nomenclature

A_a aperture area of the collector

A_r absorber area of the collector

a_c isentropic compressor pressure ratio

a_t isentropic turbine pressure ratio

C solar collector concentration ratio

c_w specific heat of the working fluid

f solar share

G solar irradiance

h_1 radiation heat loss coefficient for the solar collector

h_2 effective convection and conduction loss coefficient for the solar collector

$\dot{m}$ mass flow rate of the working substance

$\dot{m}_f$ fuel mass flow rate

P power output

$|\dot{Q}_{\mathrm{H}}|$ total heat-transfer rate absorbed from the working fluid

$|\dot{Q}_{\mathrm{HC}}|$ heat input from the combustion chamber

$|\dot{Q}'_{\mathrm{HC}}|$ heat rate transferred from the combustion chamber to the associated heat exchanger

$|\dot{Q}_{\mathrm{HS}}|$ heat rate input from the solar collector

$|\dot{Q}'_{\mathrm{HS}}|$ heat rate transferred from the solar collector to the associated heat exchanger

$|\dot{Q}_{\mathrm{L}}|$ heat-transfer rate between the working fluid and the ambient

Q_{LHV} lower heating value of the fuel

r_e fuel conversion rate

r_p overall pressure ratio

T_{HC} working temperature of the combustion chamber

T_{HS} working temperature of the solar collector

T_{L} ambient temperature (K)

T_x working fluid temperature after the heat input from the regenerator

$T_{x'}$ working fluid temperature after heat input from the solar collector

T_y working fluid exhaust temperature

T_3 turbine inlet temperature

U_{L} convective losses of the solar collector

α effective emissivity

η overall thermal efficiency

η_C combustion chamber efficiency

η_{H} thermal efficiency of the Brayton heat engine

$\varepsilon_{\mathrm{HC}}$ combustion chamber heat exchanger efficiency

$\varepsilon_{\mathrm{HS}}$ solar collector heat exchanger efficiency

η_S solar collector efficiency

η_0 effective transmittance-absorptance product

ε_c isentropic efficiency of the compressor

ε_L cold side heat exchanger efficiency

ε_r regenerator effectiveness

ε_t isentropic efficiency of the turbines

γ adiabatic coefficient of the working fluid

ρ_{H} irreversibilities due to pressure drops in the heat input

ρ_L irreversibilities due to pressure drops in the heat release

σ Stefan-Boltzmann constant

τ_{HS} temperature ratio associated to the solar collector

τ_{HC} temperature ratio associated to the combustion chamber

1 Introduction

Power generation based on gas turbine technology has experienced an enormous evolution since the first industrial gas turbines built about 1940 [1]. Directly fired coal combustion with a poor efficiency and large carbon emissions has evolved towards more complex, clean, and efficient systems. Moreover, renewable energy resources has been included in the way heat is generated in the thermodynamic cycle that the plant runs [2–4]. Gas turbines are very versatile and can operate directly or indirectly fired [5]. This fact makes them specially suitable for their integration in heat generation plants as thermosolar ones. Another key advantage is their reduced water requirements, much lower than for instance Rankine based plants, that also admit solarization. This is essential in arid regions with favorable solar irradiance conditions [6]. These power plants can be combined with other cycles in order to take advantage for instance of residual heat through heat recovery steam generators (HRSG) [7–10].

During the last years several projects have tried to develop a hybrid solar gas turbine technology in which concentrated solar power [11–13] coming from a central receiver solar plant is used to heat pressurized air that from the thermodynamic viewpoint performs a Brayton cycle [14–17]. The term hybrid refers to the fact that in low solar radiation periods (by night or when weather conditions are not favorable) a combustion chamber ensures an stable power release to the electricity grid and avoids the use of storage systems. Basic hybridization strategies are serial or parallel. In the serial scheme compressed air is pre-heated before going into the combustion chamber. The air pre-heating reduces the amount of fuel (and so, pollutant emissions) required to attain the desired turbine inlet temperature. In the parallel scheme the air flow after compression is divided in two streams, one is guided to the solar subsystem and the other is independently directed to the combustion chamber. Then, the two streams are mixed before the expansion in the turbine. This scheme has some practical advantages (operation and maintenance), but thermodynamically, the serial configuration is more profitable [18]. Hybridization can be performed by retrofitting an existing standard fossil plant of designing an original hybrid one [19]. Usually there is more flexibility in designing and optimizing a brand new one, solving the design challenges properly. It is thus required to simulate the hybrid system, taking into account techno-economic and thermo-economic ingredients [10,18,20].

According to the type of combustion (and so, to the type of fuel to be burned) solar hybridization can be done on directly fired gas turbines (DFGTs) and externally fired gas turbines (EFGTs). In the first the fuel is burned directly on the air stream and flue gases are conducted to turbine blades. In consequence, the fuel used should be clean to avoid fouling problems. The main value of DFGTs is that can reach high turbine inlet temperatures and thus, good power output. In EFGTs hot gases after combustion are not in direct contact with turbine blades [5,21]. Heat is transferred to the working fluid (air) by means of a high temperature heat exchanger (HTHE) [22]. In this case two main advantages should be mentioned: the flexibility in the plant operation, that could be in open or closed cycles, and the flexibility in the type of fuel (solid, liquid or gas, from fossil resources or renewable ones). The main drawback are heat exchangers, particularly the cost and efficiency of the HTHE at the hot side and the required cooler in the cool side if the cycle is closed to recover the compressor inlet temperature.

Apart from R+D projects, prototypes, and experimental installations several research works have been published in the last times. Some of them, make use of commercial simulation environments, (TRNSYS®, Thermoflex®, EES®, etc.) that allow a detailed description of all plant components and specific calculations on the solar subsystem [23,24]. With respect to the latter, exhaustive computations for the solar efficiency including mirror area, blocking and shadowing effects, mirror tracking strategies, and so on are accomplished [25–27]. Moreover, the utilization of meteorological databases allows to simulate the plant in particular locations and for realistic weather conditions. However, it is not easy to extract direct physical information about the main losses sources in the plant and to plan global strategies for the optimization of the plant design and operation as a whole.

On the other side, there are several theoretical works that starts from the Brayton ideal cycle and thereafter refinements are included in the analysis of the thermodynamics of the cycle in order to recover realistic output records [28–31]. Usually, in these works the model for the concentrated solar subsystem, although including the main heat transfer losses, is simple. This allows to obtain closed analytical expressions for thermal efficiencies and power output, and then check the model predictions with validation purposes for particular design point conditions, with fixed values of solar irradiance and ambient temperature. And in a possible step forward to suggest and guide optimization strategies.

The main objectives of this work are aligned in the last *modus operandi*, but with a noticeable novelty, to develop a dynamic model that allows the incorporation of solar irradiance and ambient temperature fluctuations at a particular location. We shall present a thermodynamic model for a serial solar hybrid Brayton type plant working either in recuperative or non-recuperative configurations because of the key importance of recuperation [6,31,32]. The model, in which refers to the thermodynamic cycle starts from a closed Brayton cycle however incorporating the main losses sources: non-ideal turbine and compressor, pressure decays, heat exchangers, heat transfer losses in the solar collector, combustion inefficiencies, etc. The combination of the models for the solar part and the thermodynamic engine allows to obtain expressions for the plant global efficiency and other efficiencies in terms of a reduced number of parameters, with clear physical meaning each. It will be shown that the comparison of the model predictions with real plant data at particular conditions is good. Moreover, we shall present a complete analysis of the evolution of plant records along a year, taking real data for solar irradiance and ambient temperature for representative days of each season. Particularly, fuel consumption and greenhouse emissions will be estimated and analyzed.

2 Thermodynamic plant model

We consider the plant sketched in Fig. 1. A single step regenerative closed Brayton cycle is hybridized in the following sequence. The working fluid at the compressor exit (temperature T_2) is heated up through a regenerator that makes use of the high temperature of the gas after the turbine, T_4. The temperature of the fluid at the regenerator exit, T_x, is elevated first by the heat released by the central tower solar subsystem if solar irradiance is enough. Afterwards, the fluid reaches a higher temperature, $T_{x'}$ and then, in the last heating step, it receives an energy from a combustion chamber through another heat exchanger. The final temperature at the turbine inlet, T_3, is taken as approximately constant, so the power released by the installation to the grid is also almost unchanged during all the year. In the case of insufficient irradiance a shut-off valve redirects the fluid directly to the heat exchanger below the combustion chamber. The case of no regeneration, where the fluid at the compressor exit goes directly to the heat exchanger linked to the solar receiver, will also be analyzed.

As can be seen from Fig. 1 losses in all heat exchangers, in the solar subsystem, in the combustion chamber as well as in the compressor and in the turbine will be considered. They will be specified in the following subsections. Next we detail the nomenclature for the different heat transfers in the model. The solar subsystem receives a heat input from the sun given by GA_a where G is the solar irradiance and A_a the aperture area of the solar field. The solar irradiance is a function of time because it depends on the sun position during the day, the meteorological conditions, and seasonal fluctuations. After discounting the losses, the receiver releases a useful energy to a heat exchanger, $\dot{Q}'_{\rm HS}$, that in turn releases a final heat rate $\dot{Q}_{\rm HS}$ to the working fluid.

A similar scheme is followed to describe the combustion chamber subsystem. The energy input in this subsystem is $\dot{m}_f Q_{LHV}$, where $\dot{m}_f$ is the fuel mass consumption rate and Q_{LHV} its corresponding lower heating value. The mass fuel rate will be also considered as time dependent, in accordance to the fluctuations of G. It should compensate variations in G in such a way that the turbine inlet temperature remains constant in all conditions. In the combustion chamber losses due to incomplete combustion and heat transfers to the surroundings are accounted for. The heat rate received by the working fluid from combustion of the fuel is denoted as $\dot{Q}_{\rm HC}$. The isentropic efficiencies of the heat exchangers associated to the solar and the combustion subsystems are denoted as $\varepsilon_{\rm HS}$ and $\varepsilon_{\rm HC}$ respectively. The internal heat redistribution associated to regeneration is called $\dot{Q}_r$. In order to close the thermodynamic cycle a cold-side heat exchanger is considered. The compressor inlet temperature, T_1, will depend on the external temperature, T_L, that will fluctuate due to dairy and seasonal changes. The plant delivers a mechanical power output, P, independent of solar radiation fluctuations.

2.1 Global thermal efficiency of the plant

The thermal efficiency of the whole system, η, is the ratio between the net mechanical power output, P, and the total heat input rate,

$$\eta = \frac{P}{GA_a + \dot{m}_f Q_{\rm LHV}} \tag{1}$$

The following objective is to express this global efficiency in terms of the efficiency of the solar collector, $\eta_{\rm S}$, that of the combustion chamber, $\eta_{\rm C}$, the efficiency of the Brayton heat engine, $\eta_{\rm H}$, and the efficiencies of all the required heat exchangers.

The solar collector efficiency, $\eta_{\rm S}$, is the quotient between the useful energy it delivers per unit time, $|\dot{Q}'_{\rm HS}|$ (see Fig. 1) and the solar energy rate it receives from the sun, GA_a, *i.e.*, $\eta_{\rm S} = |\dot{Q}'_{\rm HS}|/GA_a$. The working fluid undergoing the thermal cycle receives the solar heat input through a solar receiver and a heat exchanger, which transfers a fraction of $|\dot{Q}'_{\rm HS}|$, $|\dot{Q}_{\rm HS}| = \varepsilon_{\rm HS}|\dot{Q}'_{\rm HS}|$ to the working fluid. In this equation $\varepsilon_{\rm HS}$ represents the isentropic efficiency of the heat exchanger. In other terms, the solar collector efficiency can be written in terms of $\varepsilon_{\rm HS}$ and the effective heat rate released to the fluid as: $\eta_{\rm S} = |\dot{Q}_{\rm HS}|/(\varepsilon_{\rm HS} GA_a)$.

Likewise the combustion chamber generates a heat rate, $|\dot{Q}'_{\rm HC}|$, that is transferred to the working fluid by means of a heat exchanger with isentropic efficiency $\varepsilon_{\rm HC} = |\dot{Q}_{\rm HC}|/|\dot{Q}'_{\rm HC}|$, so the working fluid receives a heat rate $|\dot{Q}_{\rm HC}|$ coming from combustion. Note that we are assuming an externally fired gas turbine (EFGT), so the fuel is not injected in the air itself, but the gas receives the energy input coming from combustion through a heat exchanger. The efficiency of the combustion chamber is thus given by: $\eta_C = |\dot{Q}_{\rm HC}|/(\varepsilon_{\rm HC}\dot{m}_f Q_{\rm LHV})$.

The thermal efficiency of the heat engine itself is the fraction between the net power output, P, and the total heat input received by the working fluid, $\eta_{\rm H} = P/(|\dot{Q}_{\rm HS}| + |\dot{Q}_{\rm HC}|)$. Defining a solar share fraction as the ratio of the solar heat rate that the working fluid absorbs with respect to the total heat input, $f = |\dot{Q}_{\rm HS}|/\left(|\dot{Q}_{\rm HS}| + |\dot{Q}_{\rm HC}|\right)$ [1], the overall efficiency of the whole system, η, is obtained by substituting the definitions of η_S and η_C in Eq. (1):

$$\eta = \eta_{\rm S}\eta_C\eta_{\rm H}\left[\frac{\varepsilon_{\rm HS}\varepsilon_{\rm HC}}{\eta_C\varepsilon_{\rm HC}f + \eta_{\rm S}\varepsilon_{\rm HS}(1-f)}\right] \tag{2}$$

This expression is valid for the hybrid mode when both heat sources are simultaneously releasing energy to the fluid. In the particular case in which eventually all the energy input comes from the solar collector, $f = 1$, and $\eta = \eta_{\rm S}\eta_{\rm H}\varepsilon_{\rm HS}$, and when solar irradiance is null, and the turbine works only with the heat released in the combustion reactions, $f = 0$, and $\eta = \eta_C\eta_{\rm H}\varepsilon_{\rm HC}$.

It is also interesting to define a performance relative to the energy input with an economical cost, *i.e.*, to the fuel burned. It constitutes a *fuel conversion rate*, and can be defined as suggested by Heywood [33] for internal combustion

[1] Note that this is not the only definition of *solar share* or *solar fraction* in the literature [15,24]

engines, $r_e = P/(\dot{m}_f Q_{\rm LHV})$. It is easy to show that:

$$r_e = \frac{\eta\,\eta_S\,\eta_H\,\varepsilon_{\rm HS}}{\eta_S\,\eta_H\,\varepsilon_{\rm HS} - \eta f} \tag{3}$$

In the particular case all the energy input comes from combustion, $f = 0$, and $r_e = \eta$. In the opposite limit, if eventually all the energy was solar, $f = 1$, and $\eta = \eta_S\,\eta_H \varepsilon_{\rm HS}$, so $r_e \to \infty$. Thus, note that this rate is defined in the interval $[0, \infty]$. It does not represent a thermodynamic efficiency, it is a measure of the system performance from the viewpoint of fuel consumption costs. In a solar hybrid system as the one considered here, r_e, could get values over 1 at some point because a fraction of the energy input lacks of associated costs.

2.2 Solar subsystem and combustion process efficiencies

At low and intermediate working temperatures for the solar collector, T_{HS}, losses essentially comes from conduction and convection. At high temperatures radiation losses become significant and should be considered in any model. The energy collected at the aperture is GA_a, and the useful energy provided by the solar plant, $|\dot{Q}'_{\rm HS}|$, is the difference between the energy transmitted to the receptor, $\eta_0 GA_a$, where η_0 is the optical efficiency and the losses. These contain a linear term in temperature differences accounting for conduction and convection losses and a term on the fourth power of temperatures, linked to radiation losses. Thus, the useful heat released from the collector and its efficiency can be respectively expressed, as [34–37]:

$$|\dot{Q}'_{\rm HS}| = \eta_0\,G\,A_a - \alpha\,\sigma\,A_r\,T_L^4(\tau_{\rm HS}^4 - 1) - U_L\,A_r T_L(\tau_{\rm HS} - 1) \tag{4}$$

$$\eta_{\rm S} = \frac{|\dot{Q}'_{\rm HS}|}{GA_a} = \eta_0\left[1 - h_1\,T_L^4(\tau_{\rm HS}^4 - 1) - h_2\,T_L(\tau_{\rm HS} - 1)\right] \tag{5}$$

In these equations $\tau_{\rm HS}=T_{\rm HS}/T_L$ denotes the ratio between the working temperature of the solar receiver, $T_{\rm HS}$, and the surroundings, T_L. A_a and A_r are, respectively, the aperture and absorber areas, $h_1 = \alpha\sigma/(\eta_0 GC)$, $h_2 = U_L/(\eta_0 GC)$ are losses parameters, where U_L is the convective heat loss coefficient, α is the effective emissivity of the collector, $C=A_a/A_r$ is the concentration ratio, and σ the Stefan-Boltzmann constant. It will be considered in our model that the solar irradiance, G, and the surroundings temperature, T_L, are time functions because oscillate during a day and change with seasonal and meteorological conditions. For each particular pair of values of G and T_L at any given instant, the working temperature of the receiver, $T_{\rm HS}$, is calculated by balancing the energy received from the sun and that released to the working fluid experiencing the bottoming thermal cycle [30]. The heat released by the solar subsystem to the working fluid is $|\dot{Q}_{\rm HS}|=\varepsilon_{\rm HS}|\dot{Q}'_{\rm HS}|$, where $\varepsilon_{\rm HS}$ represents the isentropic efficiency of the corresponding heat exchanger, defined as (see Fig. 1): $\varepsilon_{\rm HS}=(T_{x'}-T_x)/(T_{\rm HS}-T_x)$.

The efficiency of the combustion chamber, $\eta_{\rm C}$, once elected the fuel to be burned and the fuel-air equivalence ratio, can be considered as a constant parameter. The heat received by the working fluid from the combustion chamber, $\dot{Q}_{\rm HC}$, can be written as:

$$|\dot{Q}_{\rm HC}| = \varepsilon_{\rm HC}|\dot{Q}'_{\rm HC}| = \varepsilon_{\rm HC}\,\eta_C\,\dot{m}_f\,Q_{\rm LHV} \tag{6}$$

By expressing the isentropic efficiency of the heat exchanger in between the combustion chamber and the thermal cycle as (see Fig. 1) $\varepsilon_{\rm HC} = (T_3 - T_{x'})/(T_{\rm HC}-T_{x'})$, the heat released, in terms of temperatures, is:

$$|\dot{Q}_{\rm HC}| = \dot{m}\,c_w\,(T_3 - T_{x'}) = \dot{m}\,c_w\,\varepsilon_{\rm HC}\,(T_{\rm HC}-T_{x'}) \tag{7}$$

where $\dot{m}$ is the working fluid mass flow and c_w is its specific heat. The effective temperature in the combustion chamber is denoted as $T_{\rm HC}$, and the associated temperature ratio as $\tau_{\rm HC} = T_{\rm HC}/T_L$. As fluctuations in G and T_L will be taken into account, the fuel mass flow to be burned in the combustion chamber will also be a time dependent function in general given by:

$$\dot{m}_f = \frac{\dot{m}\, c_w (T_3 - T_{x'})}{\eta_C\, Q_{\rm LHV}\, \varepsilon_{\rm HC}} \tag{8}$$

where $T_{x'}$ will vary with the solar irradiance and ambient conditions. The rate of fuel mass burned can be also obtained from the fuel conversion rate, r_e, as: $\dot{m}_f = P/(r_e\, Q_{\rm LHV})$.

2.3 Brayton gas-turbine efficiency

In this subsection the main assumptions considered for evaluating the the efficiency of the heat engine, $\eta_{\rm H}$, will be briefly outlined since the model have been detailed elsewhere in previous works by our group [31,32]. It is assumed that a mass rate of an ideal gas, $\dot{m}$, undergoes an irreversible closed recuperative Brayton cycle. The $T-S$ diagram of the cycle is depicted in Fig. 2, where it is stressed that both the working temperature of the solar receiver, $T_{\rm HS}$ and that of the surroundings, T_L, are fluctuating quantities. In order to obtain analytical expressions for heat transfers, a constant specific heat, c_w is assumed. Although this is a debatable hypothesis, as elsewhere commented in the literature [34], it allows to get systematic expressions, and so check the influence of the most significant parameters and extract conclusions about the main physical mechanisms that lead to losses in the plant. For numerical applications, effective values for c_w or the adiabatic coefficient, γ, will be calculated by averaging the corresponding temperature dependent polynomials,

$c_w(T)$, in the adequate temperature intervals.

(1) As starting step the gas is compressed ($1\rightarrow 2$) by means of a non-ideal compressor. Its isentropic efficiency is given by $\varepsilon_c = (T_{2s} - T_1)/(T_2 - T_1)$. In this equation T_{2s} represents the temperature of the working fluid after the compression process if it was adiabatic and T_2 is the actual temperature at the compressor outlet.

(2) Between states 2 and 3, in the most general situation, the gas receives three energy inputs in sequence. First, the non-ideal regenerator increases the gas temperature from T_2 to T_x. Its effectiveness, ε_r, is defined as the ratio between the actual temperature ($T_x - T_2$) increase and the maximum ideal one ($T_4 - T_2$): $\varepsilon_r = (T_x - T_2)/(T_4 - T_2) = (T_y - T_4)/(T_2 - T_4)$. In the case of a non-recuperative cycle, $\varepsilon_r = 0$, and in the ideal limit, $\varepsilon_r = 1$.

Secondly, the gas receives a heat flow, $|\dot{Q}_{\mathrm{HS}}|$, from the solar subsystem (step $x \rightarrow x'$) and thus its temperature increases from T_x to $T_{x'}$. Finally, the gas receives a completing heat input from the combustion chamber ($x' \rightarrow 3$) in order to ensure an approximately constant turbine inlet temperature, T_3, independently of the solar irradiance conditions.

In which respect to the pressure during the heat addition processes, a global parameter, ρ_{H}, that quantifies the pressure decrease in the process $2 \rightarrow 3$ is considered. In real plants pressure decays are associated to the particular equipment in any of the three steps of the heat input process, so the curve $2 \rightarrow 3$ would not be as smooth as it is plotted in Fig. 2. But the consideration of a unique global pressure decay parameter allows to obtain analytical equations and to numerically check the effects of pressure decays in the output parameters of the plant [24]. This parameter,

ρ_{H}, is defined as:

$$\rho_{\mathrm{H}} = \left(\frac{p_{\mathrm{H}} - \Delta p_{\mathrm{H}}}{p_{\mathrm{H}}} \right)^{(\gamma-1)/\gamma} \tag{9}$$

where p_{H} is the highest pressure of the gas and $(p_{\mathrm{H}} - \Delta p_{\mathrm{H}})$ its pressure at the turbine inlet.

(3) In the state 3 the working fluid has reached its maximum temperature and its is expanded by means of a non-ideal turbine performing the power stroke ($3 \to 4$). In Fig. 2 the state $4s$ represents the final state in the ideal case the turbine behaves isentropically, and the state 4 is the actual final state after expansion. The isentropic efficiency of the turbine, ε_t, is given by: $\varepsilon_t = (T_{4s} - T_3)/(T_4 - T_3)$.

(4) Lastly, the gas recovers the conditions at the initial state 1 by releasing heat in the process $4 \to 1$ through two steps. First, by means of the regenerator (process $4 \to y$) and later by exchanging heat to the ambient through a non-ideal heat exchanger with efficiency, ε_L (process $y \to 1$): $\varepsilon_{\mathrm{L}} = (T_1 - T_y)/(T_L - T_y)$.

The pressure loss during the whole heat release process is measured through a coefficient ρ_L given by:

$$\rho_{\mathrm{L}} = \left(\frac{p_{\mathrm{L}} - \Delta p_{\mathrm{L}}}{p_{\mathrm{L}}} \right)^{(\gamma-1)/\gamma} \tag{10}$$

where p_{L} is the gas pressure at the turbine outlet and $p_{\mathrm{L}} - \Delta p_{\mathrm{L}}$ its lowest pressure during the cycle. It is convenient to define a global pressure ratio, r_p as:

$$r_p = \frac{p_{\mathrm{H}}}{p_{\mathrm{L}} - \Delta p_{\mathrm{L}}} \tag{11}$$

Provided that the processes $1 \to 2s$ and $3 \to 4s$ are adiabatic (see Fig. 2), two parameters, a_c and a_t, related to the pressure ratios of the compressor and the turbine respectively are defined:

$$a_c = \frac{T_{2s}}{T_1} = \left(\frac{p_{\mathrm{H}}}{p_L - \Delta p_L}\right)^{(\gamma-1)/\gamma} = r_p^{(\gamma-1)/\gamma} \tag{12}$$

$$a_t = \frac{T_3}{T_{4s}} = \left(\frac{p_{\mathrm{H}} - \Delta p_{\mathrm{H}}}{p_L}\right)^{(\gamma-1)/\gamma} \tag{13}$$

From Eqs. (9), (10), and (11) it is easy to find a relationship between them, $a_t = a_c \rho_{\mathrm{H}} \rho_L$.

Once, the main hypothesis and parameters have been made explicit, we express the temperatures of all the states in the cycle in terms of the temperature of the solar collector, T_{HS}, that of the combustion chamber, T_{HC}, and the pressure ratios of the compressor, a_c and the turbine, a_t. By using the definitions in the section above, it is possible to obtain the following set of equations:

$$T_1 = \varepsilon_L T_L + T_y \left(1 - \varepsilon_L\right) \tag{14}$$

$$T_2 = T_1 + \frac{1}{\varepsilon_c}\left(T_{2s} - T_1\right) = T_1 Z_c \tag{15}$$

$$T_3 = \varepsilon_{\mathrm{HC}} T_{\mathrm{HC}} + T_{x'} \left(1 - \varepsilon_{\mathrm{HC}}\right) \tag{16}$$

$$T_4 = T_3 - \varepsilon_t \left(T_3 - T_{4s}\right) = T_3 Z_t \tag{17}$$

$$T_x = \varepsilon_r T_4 + T_2 \left(1 - \varepsilon_r\right) \tag{18}$$

$$T_y = \varepsilon_r T_2 + T_4 \left(1 - \varepsilon_r\right) \tag{19}$$

$$T_{x'} = \varepsilon_{\mathrm{HS}} T_{\mathrm{HS}} + T_x \left(1 - \varepsilon_{\mathrm{HS}}\right) \tag{20}$$

The equations (15) and (17) were simplified by introducing two definitions:

$$Z_c = 1 + \frac{1}{\varepsilon_c}\left(a_c - 1\right) \tag{21}$$

$$Z_t = 1 - \varepsilon_t \left(1 - \frac{1}{a_t}\right) \tag{22}$$

By simultaneously using Eqs. (14)-(20) it is feasible to express all the temperatures in terms of the temperatures of the heat sources, T_{HS} and T_{HC}, the ambient temperature, T_L, the pressure ratio, r_p and all the irreversibility parameters defined above. The following closed set of expressions is obtained:

$$T_2 = \frac{(1-\varepsilon_L)(1-\varepsilon_r)[\varepsilon_{\rm HC}T_{\rm HC}+\varepsilon_{\rm HS}T_{\rm HS}(1-\varepsilon_{\rm HC})]+\varepsilon_L T_L\left[Z_t^{-1}-(1-\varepsilon_{\rm HC})(1-\varepsilon_{\rm HS})\varepsilon_r\right]}{\left[Z_c^{-1}-(1-\varepsilon_L)\varepsilon_r\right]\left[Z_t^{-1}-(1-\varepsilon_{\rm HC})(1-\varepsilon_{\rm HS})\varepsilon_r\right]-(1-\varepsilon_{\rm HC})(1-\varepsilon_{\rm HS})(1-\varepsilon_L)(1-\varepsilon_r)^2} \tag{23}$$

$$T_4 = \frac{[\varepsilon_{\rm HC}T_{\rm HC}+\varepsilon_{\rm HS}T_{\rm HS}(1-\varepsilon_{\rm HC})]\left[Z_c^{-1}-(1-\varepsilon_L)\varepsilon_r\right]+\varepsilon_L T_L(1-\varepsilon_{\rm HC})(1-\varepsilon_{\rm HS})(1-\varepsilon_r)}{\left[Z_c^{-1}-(1-\varepsilon_L)\varepsilon_r\right]\left[Z_t^{-1}-(1-\varepsilon_{\rm HC})(1-\varepsilon_{\rm HS})\varepsilon_r\right]-(1-\varepsilon_{\rm HC})(1-\varepsilon_{\rm HS})(1-\varepsilon_L)(1-\varepsilon_r)^2} \tag{24}$$

$$\begin{aligned}\frac{T_3}{T_L} &= \frac{T_4}{T_L}Z_t^{-1} = \\ &= Z_t^{-1}\frac{[\tau_{\rm HC}\varepsilon_{\rm HC}+(1-\varepsilon_{\rm HC})\varepsilon_{\rm HS}\tau_{\rm HS}]\left[Z_c^{-1}-(1-\varepsilon_L)\varepsilon_r\right]+\varepsilon_L(1-\varepsilon_{\rm HC})(1-\varepsilon_{\rm HS})(1-\varepsilon_r)}{\left[Z_c^{-1}-(1-\varepsilon_L)\varepsilon_r\right]\left[Z_t^{-1}-(1-\varepsilon_{\rm HC})(1-\varepsilon_{\rm HS})\varepsilon_r\right]-(1-\varepsilon_{\rm HC})(1-\varepsilon_{\rm HS})(1-\varepsilon_L)(1-\varepsilon_r)^2}\end{aligned} \tag{25}$$

$$\frac{T_1}{T_L} = \frac{\varepsilon_L + Z_t\left(1-\varepsilon_L\right)\left(1-\varepsilon_r\right)\frac{T_3}{T_L}}{1-\varepsilon_r\left(1-\varepsilon_L\right)Z_c} \tag{26}$$

$$\frac{T_x}{T_L} = \frac{T_4}{T_L}\varepsilon_r + \frac{T_2}{T_L}\left(1-\varepsilon_r\right) = \frac{T_3}{T_L}Z_t\varepsilon_r + \frac{T_1}{T_L}Z_c\left(1-\varepsilon_r\right) \tag{27}$$

It is easy to get the temperature of the working fluid at the recuperator exit, T_y, by substituting Eqs. (23) and (24) in Eq. (19). The total heat input rate, $|\dot{Q}_{\rm H}|$, and, the heat release, $|\dot{Q}_L|$, are expressed in terms of the temperatures in the following way:

$$|\dot{Q}_H| = |\dot{Q}_{\rm HS}| + |\dot{Q}_{\rm HC}| = \dot{m}c_w\left(T_3 - T_x\right) \tag{28}$$

$$|\dot{Q}_L| = \dot{m}c_w\left(T_y - T_1\right) \tag{29}$$

where,

$$|\dot{Q}_{\rm HS}| = \dot{m}c_w\left(T_{x'} - T_x\right) = f|\dot{Q}_H| \tag{30}$$

$$|\dot{Q}_{\rm HC}| = \dot{m}c_w\left(T_3 - T_{x'}\right) = (1-f)|\dot{Q}_H| \tag{31}$$

Thus, the power output released by the heat engine, $P = |\dot{Q}_{\rm H}| - |\dot{Q}_L|$, and its thermal efficiency, $\eta_{\rm H} = P/|\dot{Q}_{\rm H}|$, have analytical expressions susceptible to be evaluated for any particular parameters arrangement. And so, from the considered models for the solar and the combustion chamber subsystems, it is possible to obtain the overall plant efficiency from Eq. (2).

It is important to stress at this point that the solar share, f, in our work does not appear as an independent parameter, but it is a function of the temperatures of the heat sources, G and solar collector details, and all the other parameters. Moreover, as a consequence of the assumptions made in this model for the sequence of heat absorption processes, the following inequalities for temperatures hold (see Fig. 2):

$$T_3 \geq T_{x'} \geq T_x \tag{32}$$

$$T_{\mathrm{HS}} \geq T_x \tag{33}$$

$$T_{\mathrm{HC}} \geq T_{x'} \tag{34}$$

Equation (32) is trivially obtained from Eqs. (30) and (31). The particular case $T_3 = T_{x'}$ holds when solar radiation is capable to provide enough energy to increase gas temperature from T_x to T_3. In terms of the solar share, $f = 1$. The equality $T_{x'} = T_x$ appears in the opposite case, all the energy comes from combustion, so the solar share is zero (by night or for very poor irradiance conditions). The other equations, Eqs. (33) and (34), arise because efficiencies of the heat exchangers, $\varepsilon_{\mathrm{HS}} > 0$ and $\varepsilon_{\mathrm{HC}} > 0$. The equalities holds in the case of ideal heat exchangers with no losses, $\varepsilon_{\mathrm{HS}} = 1$ and/or $\varepsilon_{\mathrm{HC}} = 1$.

3 Numerical implementation and validation

3.1 Validation in design point conditions

The model presented in this work was validated in fixed solar irradiance conditions in a previous paper [30]. In this section we outline the main background and conclusions of the numerical validation. As validation target it was elected the central tower concentrating collector developed by Abengoa Solar near Seville, Spain, under the project called SOLUGAS [17]. In this project, a commercial recuperative natural gas turbine (*Mercury 50*, Caterpillar) [38], was placed at the top of a 75 m high tower behind the receiver. The main objective of the installation is to check the performance and the costs estimate of this plant scheme at a pre-commercial stage. Within this aim an heliostat field consisting of 69 units of 121 m^2 reflective area each, with an innovative tracking system was built. It can produce about 5 MWth.

The validation process is divided in two steps. First, we tried to reproduce the main performance records of the turbine *Mercury 50*, for which the manufacturer provides several specifications [38]. Table 1 summarizes some data required to run our simulation as well as the measured and calculated values. We considered as working fluid air, with average values of the constant pressure specific heat, c_w and adiabatic coefficient, γ. Polynomial fits from the literature [39] were integrated over the interval $[T_1, T_3]$. The required losses parameters were assumed from standard values. Computations lead to fairly good agreement with manufacturer's measures. It is noteworthy that the relative deviations of efficiency at generator terminals, η_{He}, and power output, P_e, are below 1%. In [30] we also presented the explicit comparison of our predictions for the evolution of power output, thermal efficiency, and heat rate as functions of the ambient temperature with those provided by the manufacturer (see Fig. 4 in [30]). Also, results are quite satisfactory.

Second, it is more difficult to perform the same direct comparison for the whole plant working in hybrid conditions. This is due to the wariness of the companies developing R+D facilities of this type to make accesible details about the main parameters of the installations and the measured performance records. So, it is necessary to survey data for the required input parameters from different sources and present a prediction of the results of the model to check its credibility. This is done, in the case of our work, in Table 2. Input data were taken mainly from SOLUGAS (Abengoa Solar) project reports [17], the work by Romero *et al.* [11] but also from several other resources [21,22,34,40]. The design point conditions were taken from Abengoa at $G = 860$ W/m^2 and $T_L = 288K$. The optical efficiency, $\eta_0 = 0.73$ was taken from [11] for such design point conditions. The working temperature of the solar receiver, $T_{\rm HS}$, was obtained by matching the heat rate released by the solar collector, Eq. (4), and the input absorbed by the working fluid, Eq. (30). For the selected set of parameters this leads to $T_{\rm HS} = 1085$ K that is a reasonable value. For the lower heating value of natural gas a value of $Q_{\rm LHV} = 47.141$ MJ/kg [41] was taken. The estimated efficiencies shown at the bottom of Table 2 are in right accordance with published values for this kind of plants [11,13].

3.2 Numerical implementation of daily variations

Irradiance, G, and ambient temperature, T_L, were taken from the database by Meteosevilla [42] at a location very close to the installation of the project

SOLUGAS, Sanlúcar La Mayor, Seville, Spain. We elected data each half an hour from four regular days, each corresponding to the beginning of a season (21st): march, june, september, and december. No smoothing or averaging procedures were followed. The curves for G and T_L are represented in Fig. 3. Seville has a priori quite favorable solar conditions. The upper panel of the figure shows that the maximum value of G reached in summer is about 875 W/m^2. The maximum of the less favorable month, december reaches about 480 W/m^2. The number of insolation hours is quite elevated. At the same time temperatures are relatively high. They reach maximum values around 34°C during the day in september (in september, at the end of summer, temperatures are higher than in june) and minimum values about 4°C.

For each pair of values of G and T_L the working temperature of the collector, T_{HS} was calculated. It is difficult to find analytic expressions of the variations of the optical efficiency for a particular heliostat field [23], because η_0 depends on the actual concentrator and receiver geometry and optics. In consequence, trying to maintain the simplicity and analytical equations for heat transfers and efficiencies we preferred to take a realistic yearly averaged value of η_0. The numerical value was taken from the work by Romero *et al.* [11] for a similar facility, $\eta_0 = 0.65$.

Another important point is the one related to the pressure losses across the ducts in the plant. These losses depend of the operation regime of the plant as stressed by Barigozzi *et al.* [24,43]: are higher when the plant is operating in an hybrid mode and the working fluid is conducted through the solar receiver. We kept the values for ρ_H and ρ_L taken in the validation procedure (see Table 1) because they are quite pessimistic (represent pressure losses about 9%).

In the next sections, results with plant configurations either incorporating a regenerator or not will be shown. When no recuperator is included, investments costs are reduced, thermal efficiency decreases, and fuel consumption is higher. But temperature of the working fluid at the exit of the expansion process is high and so, the cycle is susceptible to be combined with a bottoming cycle. In the opposite situation, when an extra investment is made in the plant and a recuperator is incorporated in the design, fuel costs decrease and thermal efficiency increases, but the temperature at the regenerator exit could make more difficult to use residual heat for bottoming cycles. Moreover, the inclusion of a recuperator will be only beneficial for not too high values of the compressor pressure ratio as discussed elsewhere in the literature [6,31,32]. Both configurations will be analyzed in this work.

4 Daily basis plant records prediction

One of the key objectives of the hybridization scheme we have followed for the plant is to guarantee a power output independent of solar irradiance fluctuations. Thus, before analyzing other output records we have evaluated the evolution of P with time for days representative of each season. In Fig. 4 the particular evolution of P during a whole day is depicted for two seasons and a recuperative configuration: winter and summer (for the other two seasons and also for non-recuperative configurations conclusions would be similar). In both seasons power output oscillates with ambient temperature following a counterphase routine and is independent of the evolution of G . It is a well-known fact in gas turbines that an ambient temperature increase provokes a power output reduction and opposite. Barigozzi *et al.* [10] mention that for a temperature increase of 10°C power output decreases about 5-13% for a simple gas turbine. Several technical procedures have been proposed in the literature in order to control and avoid if necessary these oscillations [10]. Thus, in our case, power output increases during the night as T_L decreases, reaching a maximum around sunrise, and then decreases when T_L increases, and display a minimum when T_L is maximum (compare the curves for winter and summer on the bottom panel of Fig. 3 with Fig. 4). To have a quantitative idea of the amplitude of the oscillations, we have computed the relative amplitude of the oscillations defined as $(P_{\rm max} - P_{\rm min})/P_{\rm min}$. It is around 4.7% in winter (for a difference between minimum and maximum values of T_L about 11 K) and around 6.8% in summer (temperature difference about 14 K). Average value of P is slightly higher in winter (4.5% higher than in summer). So, we can conclude that power output is independent of the particular conditions of solar irradiance and is only function of ambient temperature.

4.1 Plant efficiencies

We have obtained the curves for the different thermal plant efficiencies for a representative day of each season in terms of the UTC time for two plant configurations (see Fig. 1): recuperative ($\epsilon_r = 0.775$) and non-recuperative ($\epsilon_r = 0$). These efficiencies are plotted in Figs. 5 (no regeneration is considered) and 6 (including a regenerator). The efficiency of the solar subsystem, η_S, is only defined when the solar irradiance is enough to deliver an effective heat to the working fluid, so the corresponding curves are defined for a particular time interval. For any season these curves present a wide plateau during the hours with good insolation and then η_S decreases during sunrise and sun-set. The shape of the functions in these periods is only indicative because a particular model for the evolution of the solar receiver temperature with G during transients should be necessary. This is out of the scope of this work. The plateaus are associated to the fact that solar efficiency are governed by the optical efficiency, η_0, that we considered as constant. The influence of heat losses is small in the shape of η_S, specially in the non-regenerative case (see Fig. 5), only the height of the plateaus is sensitive to the temperature dependent heat losses, Eq. (5). Of course the plateaus are wider during summer, because of the higher number of insolation hours. Largest values of η_S are about 0.63 for the non-recuperative case and slightly smaller for the recuperative case. As we shall comment later on this is due to the fact that working temperatures of the solar collector are higher in this case and so heat transfer losses in the solar subsystem are larger.

The efficiency of the Brayton heat engine, η_H, is almost constant, day and night. It depends on the ambient temperature for a particular day but its time dependence is small in the scale of the plots in Figs. 5 and 6. In seasonal terms, η_H, is higher for lower ambient temperatures: winter and spring. Its numerical value significantly increases when incorporating a recuperator, as it should be expected. For instance in winter, in Fig. 5(a), it amounts approximately 0.28 and in Fig. 6(a) increases up to 0.40. This represents an increase about 43% which is very significant. The relative increase is approximately the same in all seasons.

The global plant efficiency, η, appears as a combination of η_S, η_H, the efficiency of the combustion process, η_C, and the effectivenesses of heat exchangers (see Eq. (2)). In the absence of insolation, η, is almost time independent and becomes close to η_H. Numerical differences appear due to the combustion inefficiencies and heat exchanger losses. When the solar receiver begins its contribution as G increases, the solar subsystem is coupled to the turbine and the combustion chamber and so, the global efficiency decreases: it presents a dip during the central hours of the day. The well width depends on the number insolation hours and its depth of the maximum values that G reaches. In the recuperative configuration, Fig. 6, of course numerical values of η are larger than for the non-recuperative, Fig. 5, one because of the important increase of η_H. For $\epsilon_r = 0$, minimum values of η change between 0.21 in summer to 0.24 in winter. For $\epsilon_r = 0.775$ the smallest value is found in summer, 0.27, and in winter is around 0.32.

Although the fuel conversion rate, r_e, thoroughly is not a thermal efficiency is also plotted in Figs. 5 and 6. It is identical to η during nights because all the heat input is associated to fuel combustion and during the day it has a parabolic shape that resembles the shape of G and qualitatively is like a mirror image of η. The maximum value of r_e appears in summer, when irradiance reaches its higher values: for $\epsilon_r = 0$. It amounts 0.34 and for $\epsilon_r = 0.775$, 0.53 which is a quite interesting value. In the less favorable season, winter, it amounts 0.30 without recuperation and 0.45 with recuperation.

The solar share, f, was defined in Sec. 2 as the ratio between the input heat rate from the solar collector and the total input heat rate. Its evolution with time for the considered representative days is plotted in Fig. 7. Curves for recuperative and non-recuperative configurations are shown. In all cases the shape of f for any particular season reminds that of the solar irradiance, G. Differences among seasons refer both to the number of hours with enough solar irradiance and to the height of the curves maxima. For instance in winter for the regenerative configuration f reaches a value slightly above 0.16 and there are 9 hours of effective irradiance. At the other side, for a typical day of summer, f has a maximum around 0.34 and about 14 hours of adequate solar input. When the regenerator is eliminated, for example, with the aim to take advantage of the residual heat in a bottoming cycle, the solar heat input remains the same. Nevertheless, the total heat input (in this case required to increase the temperature from T_2 to T_3 instead of from T_x to T_3) is larger, so the solar share is smaller. If we compare f in the figure for winter in both configurations, in the recuperative one the maximum is about 0.165 as mentioned above and for the non-recuperative one about 0.125. This corresponds to a decrease around 32%. At the other end, in summer the maximum with no recuperation is on 0.245, thus an increase about 39% is gained with a recuperator.

4.2 Cycle temperatures

The relevant temperatures in the hot side of the cycle are plotted in Fig. 8 for the regenerative and the non-regenerative configurations. The turbine inlet temperature, T_3, is almost constant in both configurations, thus providing an stable plant power output as commented at the beginning of Sec. 4. The compressor outlet temperature, T_2 is around 600 K and slightly oscillates following the evolution of the ambient temperature. In the non-regenerative situation and during insolation hours the solar receiver increases the temperature of the fluid from T_2 to $T_{x'}$. The latter has during these hours a parabolic shape that resembles the shape of G. During winter the maximum of $T_{x'}$ is about 700 K and during summer about 820 K. The working temperature of the solar collector, T_{HS}, as explained before is obtained, in each case, by balancing the energy rate released by the solar collector and received by the working fluid performing the Brayton cycle. It reaches maximum values above $T_{x'}$ because of the losses in the heat exchanger behind the solar receiver. The maximum values of T_{HS} in the non-regenerative situation change from 720 K in winter to 870 K in summer.

In the regenerative situation, the regenerator increases the compressor output temperature T_2 to a temperature T_x (see Fig. 1). Then, the solar collector during the day and the combustion chamber provide the heat rates to reach the turbine inlet temperature, T_3. The value of T_x does not depend neither on the time during a day nor on the season, because it is a function of the turbine outlet temperature T_4 (constant because T_3 is constant) and the regenerator effectiveness. In the plant considered T_x is around 825 K. In this case all the temperatures of the hot side (T_{HS} and $T_{x'}$) are displaced above more than 200 K. In the most favorable insolation conditions, during summer, the working temperature of the solar receiver, T_{HS} is slightly above 1000 K, similar to design point conditions of SOLUGAS project. It is important to stress here that for the intended power output in this plant $T_{x'}$ never reaches the turbine inlet temperature, T_3. This means that this plant could not work only on solar basis if the aim is to obtain a power output around 4.6 MW. A substantial combustion contribution is always required, even for the highest values of G.

The temperatures of the working fluid in the cold side are depicted in Fig. 9. This plot is interesting in order to analyze the possible combination of the Brayton cycle with a bottoming one in order to take advantage of residual heat for instance through a heat recovery steam generator (HRSG) and a Rankine cycle or other possible cycles. In the non-regenerative case the temperature of the working fluid at the turbine outlet, T_4 is season independent and is about

890 K. When a regenerator is considered, the temperature of the working fluid that could be profited is T_y. During a day T_y oscillates as T_L and it also depends on the particular season. The smallest value is found in december, about 650 K, and the largest one in september, around 675 K. Thus, differences between seasons are scarce. Both in the non-regenerative and regenerative situations the potential use of residual heat to connect a bottoming cycle are important [9,11,13,44].

4.3 Fuel consumption and emissions

Numerical computation of the fuel consumption was achieved, either calculating the fuel consumption rate in hourly basis through Eq. (8) or the integrated consumption during a whole day. The mass fuel rate, $\dot{m}_f$, (see Fig. 10) has two different levels depending on the plant configuration, with or without a heat recuperator. During the night all the electricity generation comes from fuel combustion (natural gas in our case) and differences between recuperative and non-recuperative cases are around 38.5 %, independently of the season. This is the difference in terms of fuel consumption rate of incorporating a regenerator to pre-heat the working fluid at the compressor exit. When the plant works on a hybrid mode because received irradiance is enough to heat the pressurized air above T_2 (without recuperation) or T_x (with recuperation), the fuel rate saving is important, and obviously depends on seasonal conditions. For each operation mode, the fuel saving for a whole day corresponds to the area of the surface between the solid lines in Fig. 10 (hybrid mode) and the corresponding dashed ones (pure combustion). The results are summarized in Table 3. For the non-regenerative plant the saving varies from 2.9% in winter to 8.7% in summer. Autumn and spring behave in a similar way, the saving is about 5.5%. For the recuperative case relative differences are slightly larger: change from 4.0% in winter to 11.7% in summer. In autumn and spring, now the saving is around 7.4%.

The differences among plant configurations in fuel consumption are directly transferred to pollutant emissions. As an illustration we have plotted in Fig. 11 a bar diagram with the estimated emissions of the main greenhouse gases in real units: CO_2, CH_4, and N_2O. The data in the figure should only be taken as a guide, because each plant could have particular technologies to reduce emissions or CO_2 capture mechanisms. The data were obtained from the gas natural emission factors collected in [45,46]. The figure, in daily basis for the considered particular days of each season, allow to discern two emission levels: the associated to the non-recuperative plant and the one arising from the recuperative one. Differences are substantial as was previously commented for fuel consumption. Within these two modes, the reduction associated to solar hybridization and its evolution during the year is also apparent.

5 Summary and conclusions

In this paper we have modeled a solar hybrid power plant based on a gas turbine following a closed Brayton cycle. The plant admit several configurations with or without a heat recuperator and with or without solar heat input. An assumed basic constraint of the plant operation is to keep an almost constant power output in the periods of low solar radiation. The model allows a direct calculation of the dynamic plant operation, with variable solar irradiance and variable external temperature. The hybridization scheme follows a serial or sequential heat input divided in two or three steps. In the non-recuperative configuration a heat exchanger transfers the heat received in a central tower solar collector to the working fluid at the exit of the compressor. Then, a combustion chamber completes the energy input required to have an stationary turbine inlet temperature. If a regenerator is included there exist a previous heating process by using the high temperature of the gas at the turbine exit.

The main emphasis was laid on the thermodynamic model of the Brayton cycle, where all the main irreversibility sources were considered avoiding to introduce a huge number of parameters and allowing to obtain analytical equations for all the thermal efficiencies and power output. For the solar subsystems a simple model was taken. It takes into account heat losses in the solar collector due to to radiation and conduction/convection terms. The optical efficiency is an averaged effective factor. The overall plant efficiency was obtained as a combination of the efficiency of the plant subsystems (solar, combustion, and gas turbine) and the isentropic efficiencies of the heat exchangers connecting subsystems. The Brayton cycle model was explicitly validated by comparing with the data of a commercial gas turbine. The SOLUGAS project [17] in Spain was elected as prototypical installation to compare model predictions with.

After the validation in stationary conditions, real seasonal data for solar irradiance and ambient temperature were incorporated to our computational scheme and taking representative days for each season, results were presented. Curves of global plant thermal efficiency, efficiencies of the subsystems, solar share, power output, and fuel conversion rate were shown in hourly basis. Explicit data for fuel consumption rate and greenhouse gases inventory were presented and analyzed.

Results show that a regenerative plant working in hybrid mode has a fair potential to generate power output with reduced fuel consumption and reduced greenhouse emissions. Likely, the high temperature of the working gas at the recuperator exit, make these plants susceptible to be combined with a bottoming cycle, in order to increase global combined efficiency. Future efforts will be devoted to this possibility. Also a complete exergetic analysis of this hybrid plant and a thermoeconomic study are under way.

Acknowledgements

M.J. Santos, A. Medina, and A. Calvo Hernández acknowledge financial support from MINECO of Spain, Grant ENE2013-40644-R.

References

[1] P. Walsh, P. Fletcher, Gas Turbine Perfomance, Blackwell Science Ltd., 2004.

[2] W. le Roux, T. Bello-Ochende, J. Meyer, Thermodynamic optimisation of the integrated design of a small-scale solar thermal Brayton cycle, Int. J. Energ. Res. 36 (2012) 1088–1104.

[3] M. Jamel, A. Abd Rahman, A. Shamsuddin, Advances in the integration of solar thermal energy with conventional and non-conventional power plants, Rene. Sust. Energ. Rev. 20 (2013) 71–81.

[4] E. Jansen, T. Bello-Ochende, J. Meyer, Integrated solar thermal Brayton cycles with either one or two regenerative heat exchangers for maximum power output, Energy 86 (2015) 737–748. doi:10.1016/j.energy.2015.04.080.

[5] K. Al-Attab, Z. Zainal, Externally fired gas turbine technology, Appl. Energ. 138 (2015) 474–487.

[6] M. Dunham, B. Iverson, High-efficiency thermodynamic power cycles for concentrated solar power systems, Renew. Sust. Energ. Rev. 30 (2014) 758–770.

[7] M. Ahmed, H. Mohamed, Performance characteristics of modified gas turbine cycles with steam injection after combustion exit, Int. J. Energ. Res. 36 (2012) 1346–1357.

[8] M. Ghazikhani, M. Passandideh-Fard, M. Mousavi, Two new high-performance cycles for gas turbine with air bottoming, Energy 36 (2011) 294–304.

[9] R. Chacartegui, J. Muñoz de Escalona, D. Sánchez, B. Monje, T. Sánchez, Alternative cycles based on carbon dioxide for central receiver solar power, Appl. Thermal Eng. 31 (2011) 872–879.

[10] G. Barigozzi, A. Perdichizzi, C. Gritti, I. Guaiatelli, Techno-economic analysis of gas turbine inlet air cooling for combined cycle power plant for different climatic conditions, Appl. Therm. Eng. 82 (2015) 57–67.

[11] M. Romero, R. Buck, E. Pacheco, An update on solar central receiver systems, projects, and technologies, Transactions of the ASME 124 (2002) 98.

[12] M. Romero, A. Steinfeld, Concentrating solar thermal power and thermochemical fuels, Energy Environ. Sci. 5 (2012) 9234–9245.

[13] O. Behar, A. Khellaf, K. Mohammedi, A review of studies on central receiver solar thermal power plants, Rene. Sust. Energ. Rev. 23 (2013) 12–39.

[14] SOLGATE. Solar hybrid gas turbine electric power system, Tech. Rep. EUR 21615, European Commission (2005).

[15] P. Schwarzbözl, R. Buck, C. Sugarmen, A. Ring, M. Marcos Crespo, P. Altwegg, J. Enrile, Solar gas turbine systems: design, cost and perspectives, Sol. Energy 80 (2006) 1231–1240.

[16] Solar-hybrid power and cogeneration plants, Tech. rep., European Commission (2011).
URL `ordis.europa.eu/publication/rcn/13318_en.html`

[17] R. Korzynietz, M. Quero, R. Uhlig, SOLUGAS-future solar hybrid technology, Tech. rep., SolarPaces (2012).
URL `http://cms.solarpaces2012.org/proceedings/paper/7ee7e32ece8f2f8e0984d5ebff9d77b`

[18] E. Okoroigwe, A. Madhlopa, Evaluation of the potential for hybridization of gas turbine power plants with renewable energy in south africa, IEEE Conferencia Publications, 2015. doi:10.1109/DUE.2015.7102985.

[19] J. Spelling, Hybrid solar gas-turbine power plants, Ph.D. thesis, KTH Royal

Institute of Technology, Department of Energy Technology, Stockholm, Sweden (2013).

[20] Y. Li, S. Liao, G. Liu, Thermo-economic multi-objective optimization for a solar-dish Brayton system using NSGA-II and decision making, Elect. Power. Energ. Sys. 64 (2015) 167–175.

[21] P. de Mello, D. Monteiro, Thermodynamic study of an EFGT (Externally Fired Gas-Turbine) cycle with one detailed model for the ceramic heat exchanger, in: Proceedings of ECOS 2011 Conference, Novi Sad, Serbia, 2011.

[22] B. Sunden, High temperature heat exchangers (HTHE), in: Proceedings of the Fifth International Conference on Enhanced, Compact and Ultra-Compact Heat Exchangers: Science, Engineering and Technology, Hoboken, NJ, USA, 2005.

[23] S. Kalogirou, Solar thermal collectors and applications, Prog. En. Comb. Sci. 30 (2004) 231–295.

[24] G. Barigozzi, G. Bonetti, G. Franchini, A. Perdichizzi, S. Ravelli, Thermal performance prediction of a solar hybrid gas turbine, Sol. Energy 86 (2012) 2116–2127.

[25] C. Noone, M. Torrilhon, A. Mitsos, Heliostat field optimization: a new computationally efficient model and biomimetic layout, Sol. Energ. 86 (2012) 792–803.

[26] F. Collado, J. Guallar, A review of optimized design layouts for solar power tower plants with *campo* code, Ren. Sust. Energ. Rev. 20 (2013) 142–154.

[27] R. Soltani, P. Keleshtery, M. Vahdati, M. KhoshgoftarManesh, M. Rosen, M. Amidpour, Multi-objective optimization of a solar-hybrid cogeneration cycle: application to CGAM problem, Energ. Conv. Manage. 81 (2014) 60–71.

[28] A. McMahan, S. Klein, D. Reindl, A finite-time thermodynamic framework for optimizing solar-thermal power plants, J. Sol. Energ. Eng. 129 (2007) 355–362.

[29] W. Le Roux, T. M. J. Bello-Ochende, A review on the thermodynamic optimisation and model of the solar thermal Brayton cycle, Renew. Sust. Energ. Rev. 28 (2013) 677–690.

[30] D. Olivenza-León, A. Medina, A. Calvo Hernández, Thermodynamic modeling of a hybrid solar gas-turbine power plant, Energ. Convers. Manage. 93 (2015) 435–447.

[31] S. Sánchez-Orgaz, A. Medina, A. Calvo Hernández, Recuperative solar-driven multi-step gas turbine power plants, Energ. Convers. Manage. 67 (2013) 171–178.

[32] S. Sánchez-Orgaz, M. Pedemonte, P. Ezzatti, P. Curto-Risso, A. Medina, A. Calvo Hernández, Multi-objective optimization of a multi-step solar-driven Brayton cycle, Energ. Convers. Manage. 99 (2015) 346–358.

[33] J. Heywood, Internal Combustion Engine Fundamentals, McGraw-Hill, 1988.

[34] L. Wu, G. Lin, J. Chen, Parametric optimization of a solar-driven Braysson heat engine with variable heat capacity of the working fluid and radiation-convection heat losses, Renew. Energ. 35 (2010) 95–100.

[35] A. Bejan, Advanced Engineering Thermodynamics, 3rd Edition, Wiley, Hoboken, New Jersey, 2006.

[36] J. Duffie, W. Beckman, Solar Engineering of Thermal Processes, John Wiley and Sons, Hoboken, New Jersey, 2006.

[37] W. Xie, Y. Dai, R. Wang, Numerical and experimental analysis of a point focus solar collector using high concentration imaging PMMA Fresnel lens, Energ. Convers. Manage. 52 (2011) 2417–2426.

[38] S. T. Caterpillar, https://mysolar.cat.com/cda/files /126873/7/dsm50pg.pdf.
URL `https://mysolar.cat.com/cda/files/126873/7/dsm50pg.pdf`

[39] K. Wark, D. Richards, Thermodynamics, 6th Edition, McGraw-Hill, 1998.

[40] Y. Zhang, B. Lin, J. Chen, Optimum performance characteristics of an irreversible solar-driven Brayton heat engine at the maximum overall efficiency, Renew. Energ. 32 (2007) 856–867.

[41] GREET, The Greenhouse Gases, Regulated Emissions and Energy Use in Transportation Model., Tech. rep., Argonne National Laboratory, Argonne, IL (2010).
URL http://greet.es.anl.gov

[42] Meteosevilla. http://www.meteosevilla.com.
URL http://www.meteosevilla.com

[43] A. Ávila-Marín, Volumetric receivers in solar thermal power plants with centra receiver system technology: a review, Sol. Energy 85 (2011) 891–910.

[44] D. Sánchez, B. Monje Brenes, J. Muñoz de Escalona, R. Chacartegui, Non-conventional combined cycle for intermediate temperature systems, Int. J. Energy Res. 37 (2013) 403–411.

[45] Direct emissions from stationary combustion sources (May 2008).
URL www.epa.gov/climateleaders

[46] Emission factors for greenhouse gas inventories (April 2014).
URL
http://www.epa.gov/climateleadership/documents/emission-factors.pdf

Mercury 50 manufacturer's specifications and output records			
$\dot{m} = 17.9$ kg/s	$r_p = 9.9$	$T_L = 288$ K	
$T_3 = 1423$ K	$T_y = 647$ K	$\eta_{He} = 0.385$	$P_e = 4.6$ MW$_e$
Model: Assumed losses parameters			
$\varepsilon_{HC} = 0.980$	$\rho_H = \rho_L = 0.975$	$\varepsilon_t = 0.885$	$\varepsilon_r = 0.775$
$\varepsilon_L = 0.985$		$\varepsilon_c = 0.815$	
Model: Estimated output records			
$T_3 = 1418$ K	$T_y = 657$ K	$\eta_{He} = 0.384$	$P_e = 4.6$ MW$_e$
Relative deviations			
T_3	T_y	η_{He}	P_e
0.4 %	1.5 %	0.2 %	0.6 %

Table 1

Manufacturer's output results for the turbine *Mercury 50* (Solar Turbines, Caterpillar) [38] and the predictions of our thermodynamic model with the irreversibility set of parameters shown. The specifications give the efficiency and power output as measured as generator terminals. In our numerical calculations, generator efficiency was taken as 0.99 %. The pressure losses parameters, ρ_H and ρ_L, correspond to relative pressure losses, both in heat input and heat release processes of 9.2%.

Solar plant parameters at design point		
$\eta_0 = 0.73$	$\varepsilon_{HS} = 0.78$	$G = 860$ W/m^2
$\alpha = 0.1$	$C = 425.2$	$U_L = 5$ W/(m^{2}K)
Combustion related parameters		
$\eta_C = 0.98$	$T_{HC} = 1430$ K	$\varepsilon_{HC} = 0.98$
Thermal cycle temperatures (K)		
$T_1 = 294$	$T_2 = 590$	$T_x = 822$
$T_{x'} = 1027$	$T_3 = 1422$	$T_4 = 890$
$T_y = 657$		
Estimated output parameters		
$f = 0.341$	$\dot{m}_f = 0.172$ kg/s	$P = 4.647$ MW
Estimated efficiencies		
$\eta_H = 0.393$	$\eta_S = 0.698$	$\eta = 0.300$

Table 2

Simulation predictions for the main parameters of the hybrid solar gas-turbine plant developed for the SOLUGAS project [17,11]. The elected parameters for the simulation of the combustion chamber and solar subsystems are shown. All other parameters for the gas-turbine itself are those contained in Table 1. The working temperature of the solar collector, T_{HS}, was obtained from an energy balance, leading to $T_{HS} = 1085$ K. The fuel conversion rate predicted is $r_e = 0.573$.

	m_f (kg per day)	Winter	Spring	Summer	Autumn
No regeneration	Combustion mode	30438	30114	29463	29196
	Hybrid mode	29552	28479	26895	27587
Fuel saving (%)		2.9	5.4	8.7	5.5
With regeneration	Combustion mode	21977	21902	21750	21688
	Hybrid mode	21098	20277	19196	20089
Fuel saving (%)		4.0	7.4	11.7	7.4

Table 3

Seasonal fuel consumption prediction on the basis of natural gas fueling. Combustion mode corresponds to the case of no solar heat input and the hybrid mode to the case in which solar irradiance is enough for partial heat input coming from the central tower solar plant.

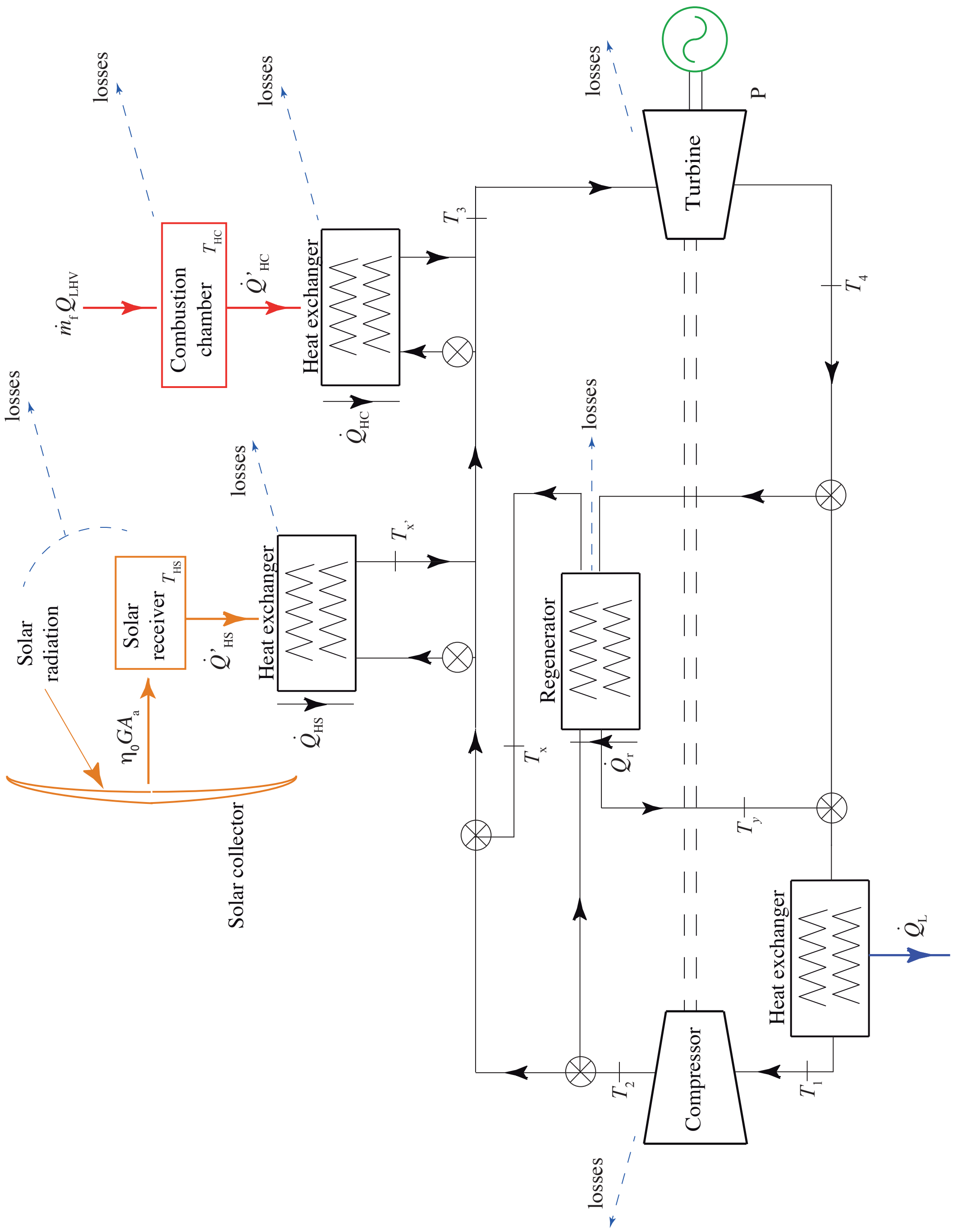

Fig. 1. Scheme of the hybrid solar gas-turbine plant considered. The main heat transfers and temperatures are depicted. Also the key losses sources considered in the model are shown. The design is flexible because the plant can work in different modes: with or without solar hybridization depending on irradiance conditions, and with or without regenerator.

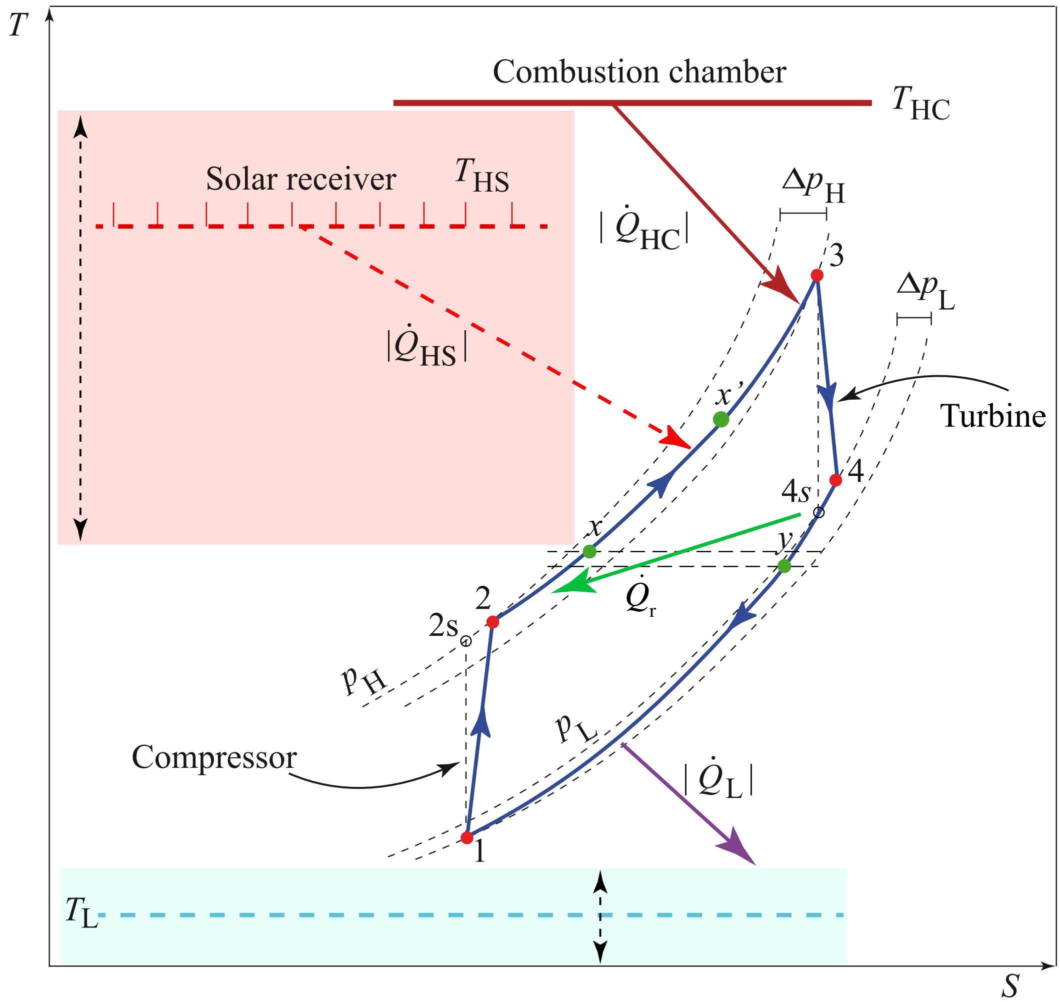

Fig. 2. $T - S$ diagram of the irreversible Brayton cycle experienced by the working fluid. Several irreversibility sources are considered (see text). The solar receiver temperature T_{HS} and the ambient temperature T_L are considered as variable parameters.

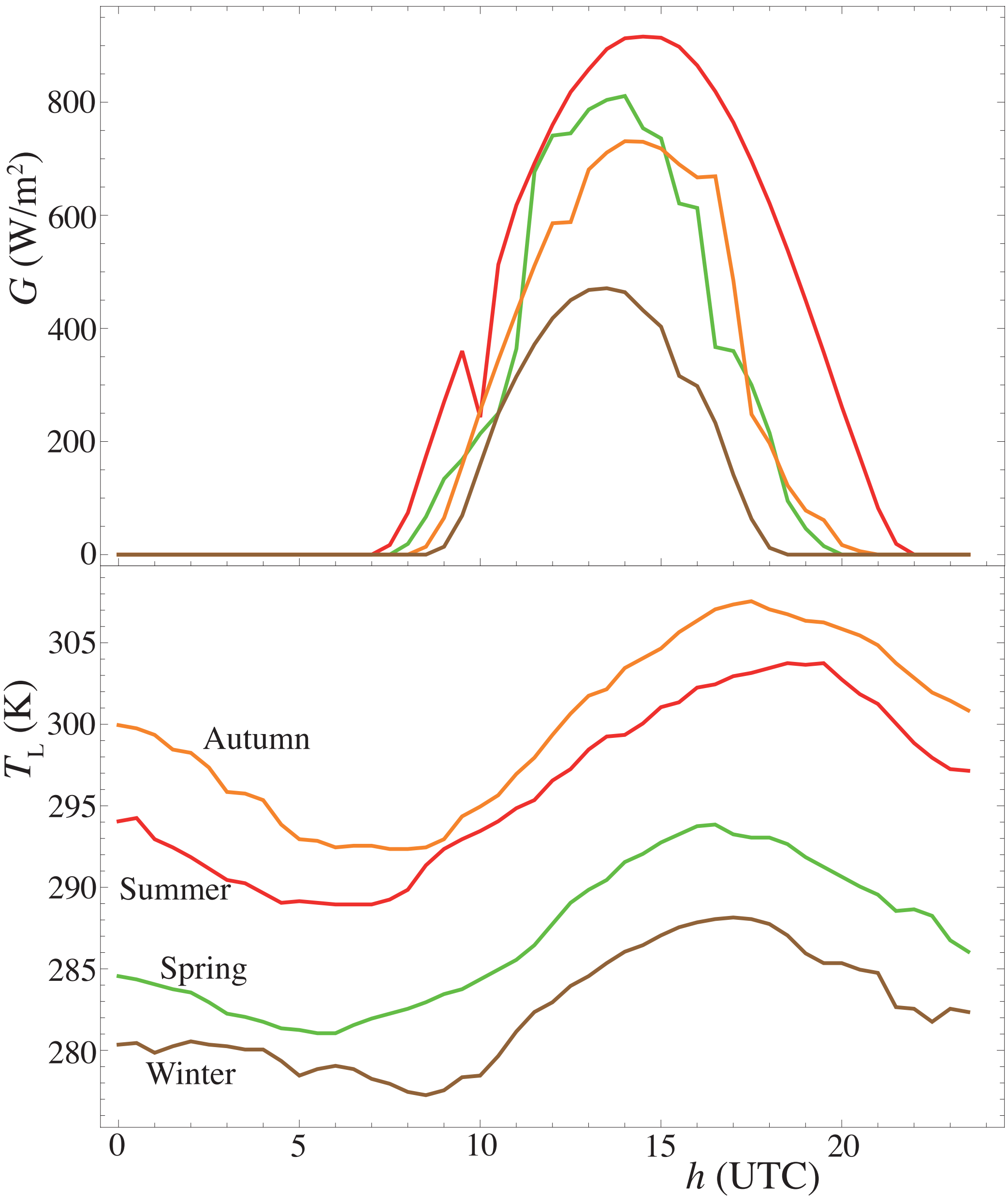

Fig. 3. Hourly Irradiance, G, and ambient temperature, T_L, for four selected days at the beginning of each season at Seville [42]. Curves are neither smoothed nor averaged. Data corresponds to direct real measures on 2013 each 30 minutes. Note that, although irradiance is higher at june (summer), temperatures at the beginning of autumn (september 21st) are higher.

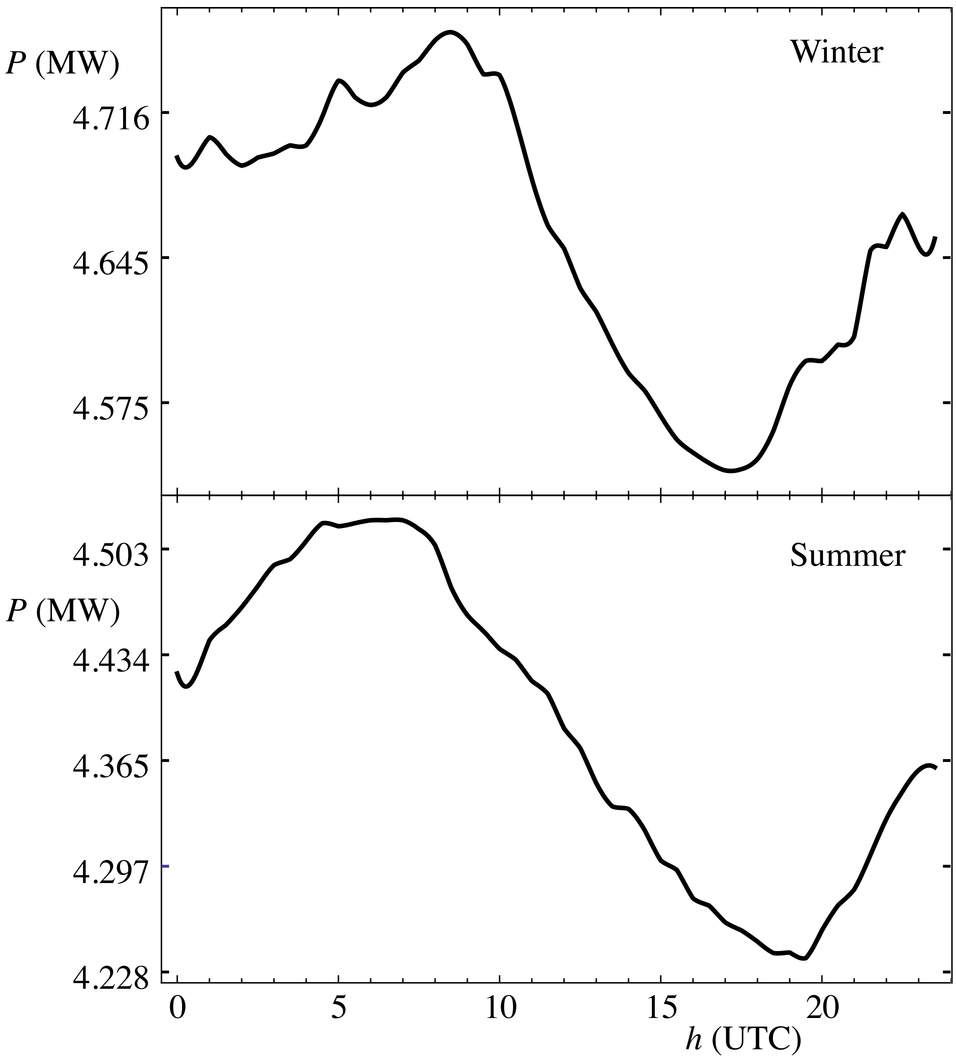

Fig. 4. Daily evolution of the power output, P, in real units. Two seasons are depicted for a recuperative plant configuration. Note that the shape of the curves resemble the counterphase shape of the ambient temperature, T_L, shown in Fig. 3, for the corresponding seasons.

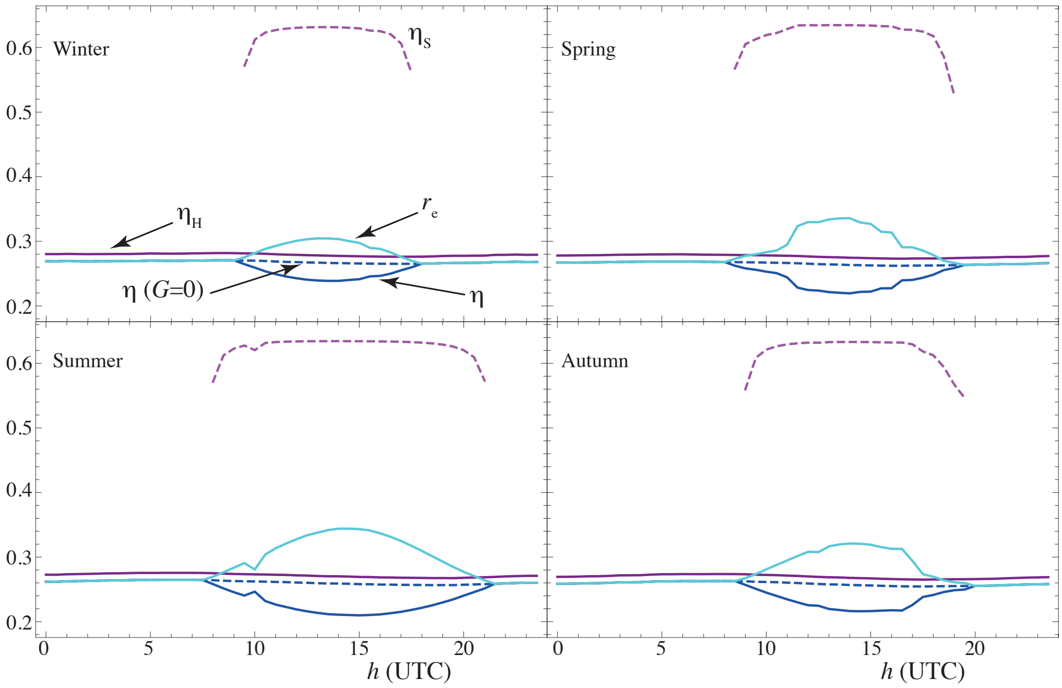

Fig. 5. Hourly evolution of plant efficiencies for representative days of each season. The plant configuration does not include recuperation ($\epsilon_r = 0$). The fuel rate conversion, r_e, although strictly not an efficiency, is also plotted (see Eq. (3)).

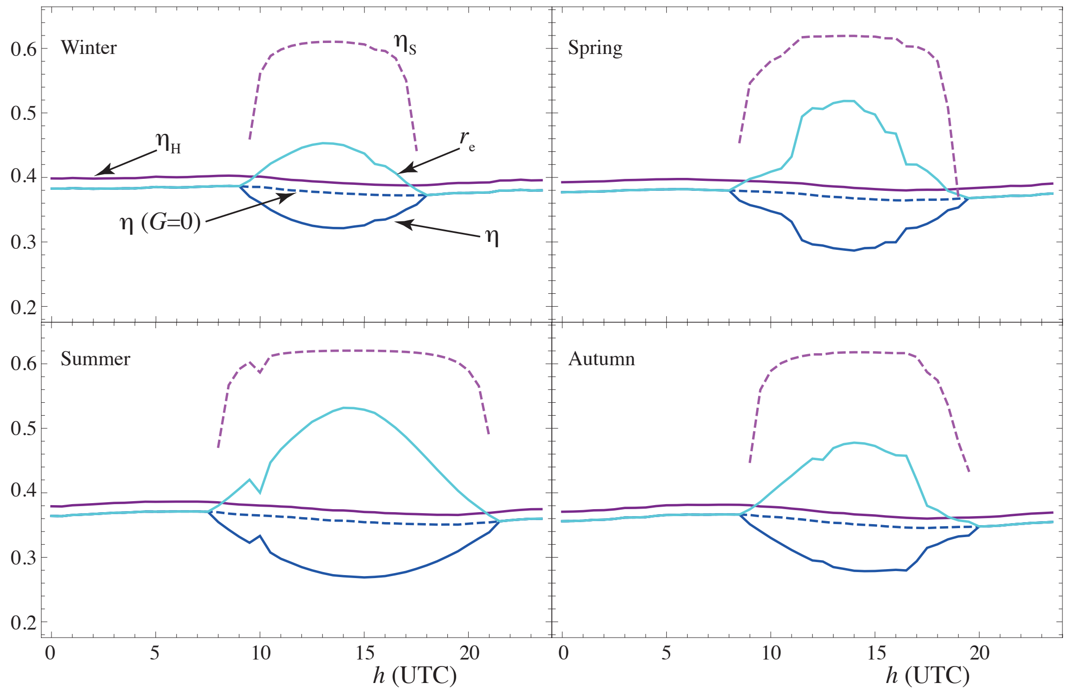

Fig. 6. Hourly evolution of plant efficiencies for representative days of each season. The plant configuration includes a regenerator with effectiveness $\epsilon_r = 0.775$.

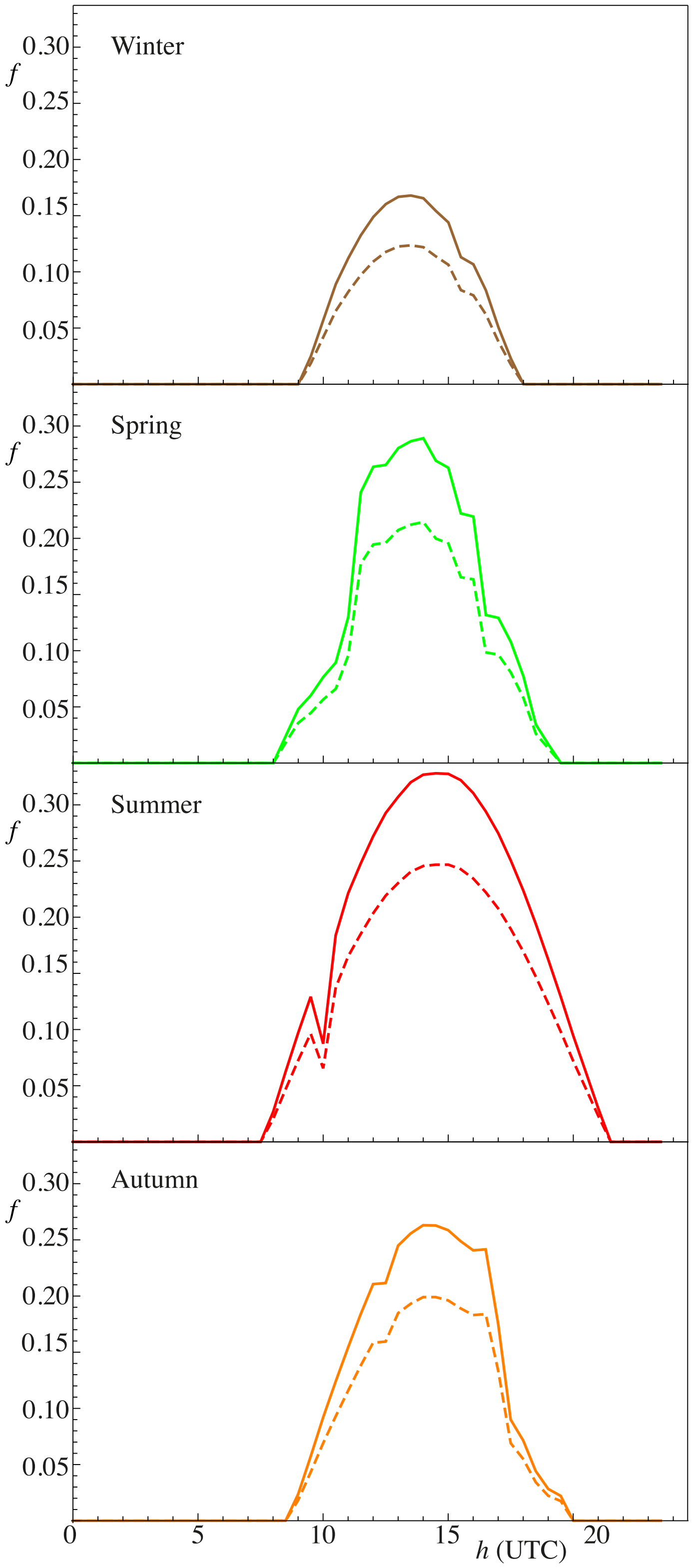

Fig. 7. Solar share, f, of the plant for each season. Solid lines correspond to the recuperative configuration and dashed lines to the non-recuperative one.

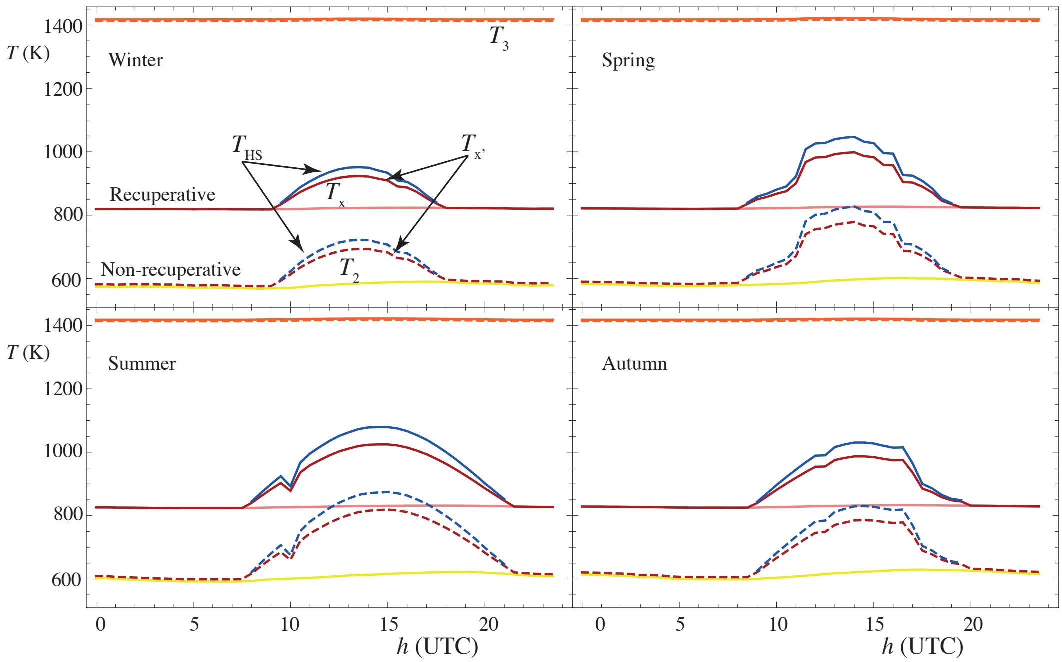

Fig. 8. Temperatures on the hot side of the plant cycle (see Figs. 1 and 2) for representative days of each season. Curves for non-recuperative and recuperative configurations are shown. The curve for T_3 is shown dashed for the non-recuperative case and solid for the recuperative.

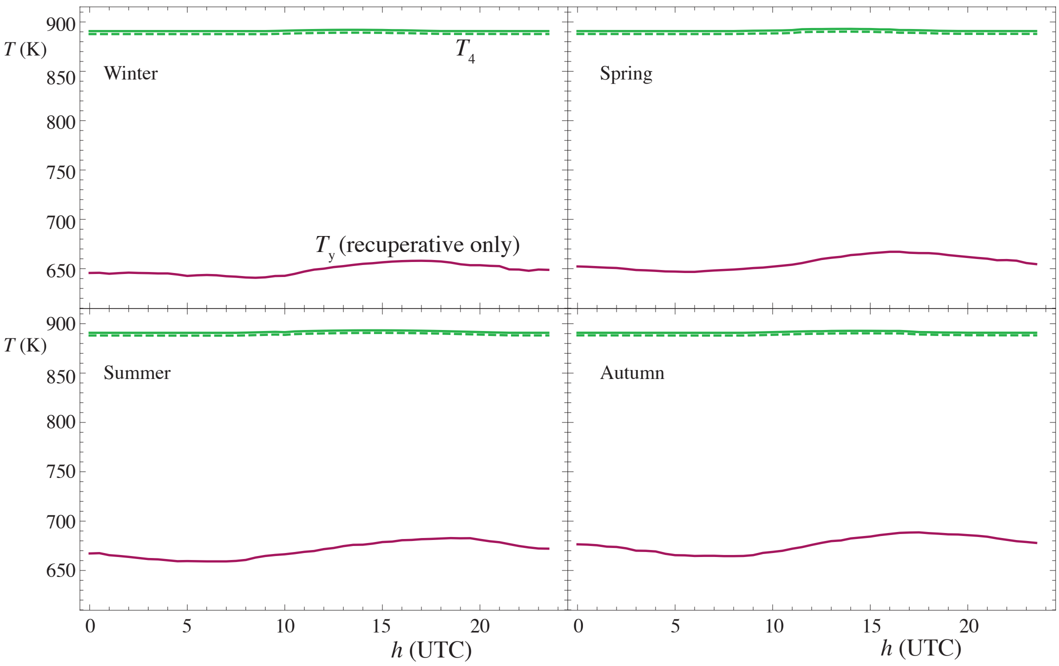

Fig. 9. Temperatures on the cold side of the plant cycle (see Figs. 1 and 2) for representative days of each season. The curve for T_4 is shown dashed for the non-recuperative case and solid for the recuperative.

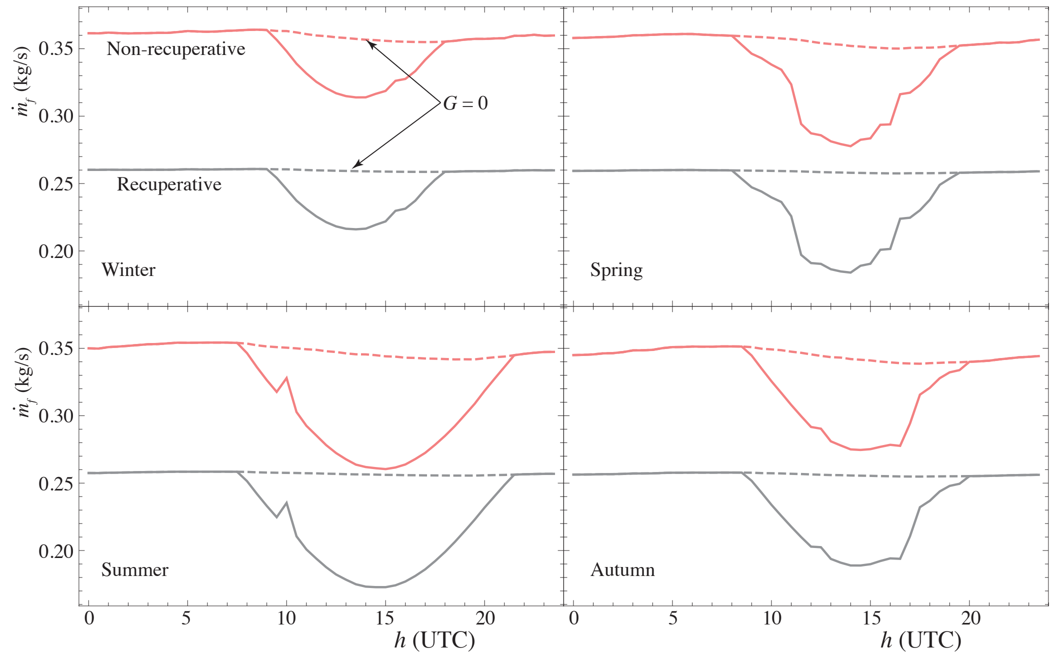

Fig. 10. Evolution with time of the fuel consumption rate, $\dot{m}_f$, supposed natural gas for representative days of each season. Solid lines refer to the hybrid operation mode and dashed ones to the pure combustion mode.

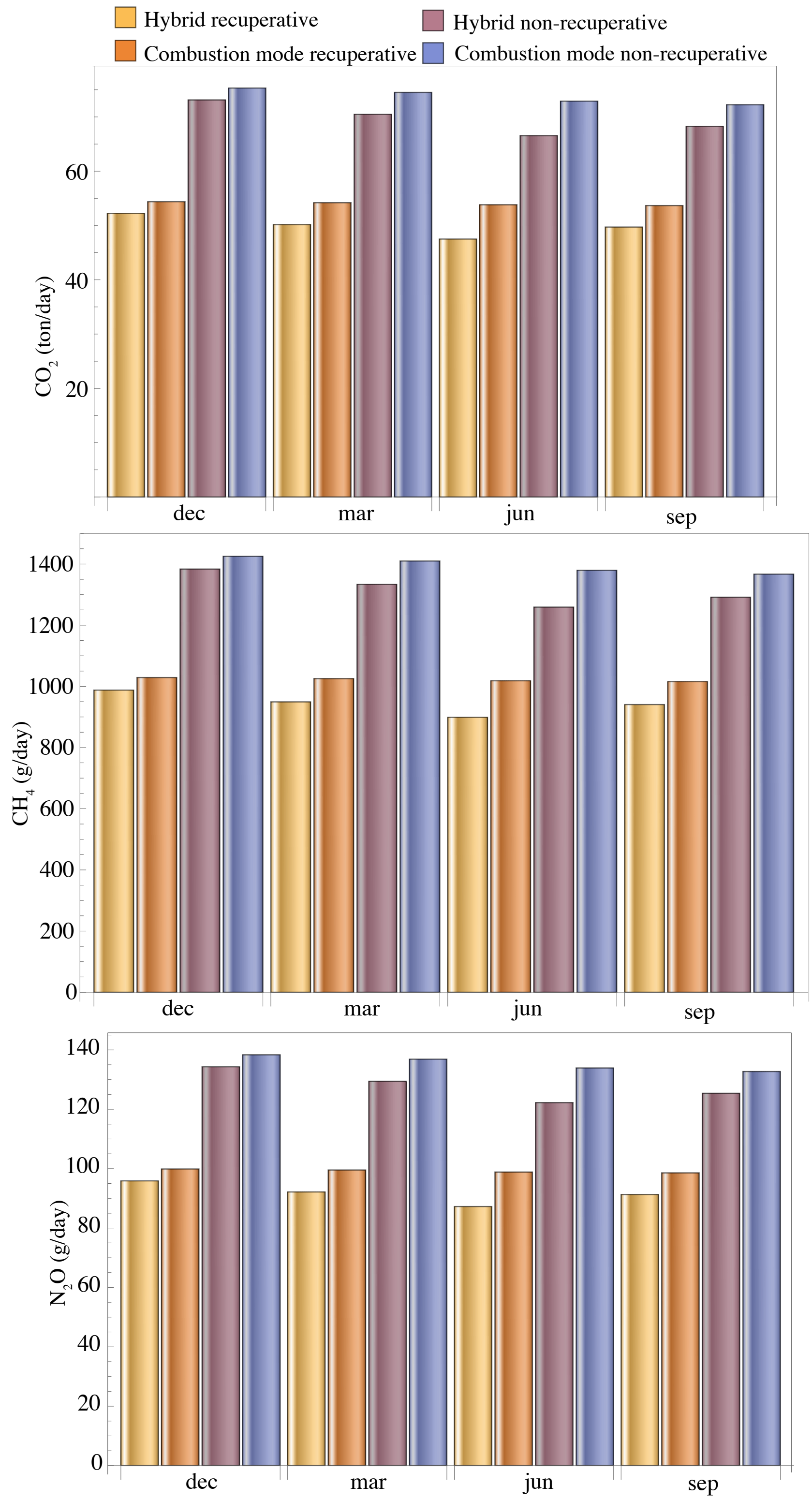

Fig. 11. Real units estimation of greenhouse emissions from the considered model. Four possible operation modes are considered: hybrid mode (partial solar heat input) with or without recuperation and pure combustion mode (only natural gas burning) with or without recuperation.